Simulation study of the coil-globule transition of a polymer in solvent

James M. Polson and Neil E. Moore
Department of Physics, University of Prince Edward Island, 550 University Avenue, Charlottetown, Prince Edward Island, C1A 4P3, Canada

(Received 28 September 2004; accepted 19 October 2004; published online 21 December 2004)

Molecular dynamics simulations are used to study the coil-globule transition for a system composed of a bead-spring polymer immersed in an explicitly modeled solvent. Two different versions of the model are used, which are differentiated by the nature of monomer-solvent, solvent-solvent, and nonbonded monomer-monomer interactions. For each case, a model parameter λ determines the degree of hydrophobicity of the monomers by controlling the degree of energy mismatch between the monomers and solvent particles. We consider a λ-driven coil-globule transition at constant temperature. The simulations are used to calculate average static structure factors, which are then used to determine the scaling exponents of the system in order to determine the θ-point values λ_θ separating the coil from the globule states. For each model we construct coil-globule phase diagrams in terms of λ and the particle density ρ. The results are analyzed in terms of a simple Flory-type theory of the collapse transition. The ratio of λ_θ for the two models converges in the high density limit exactly to the value predicted by the theory in the random mixing approximation. Generally, the predicted values of λ_θ are in reasonable agreement with the measured values at high ρ, though the accuracy improves if the average chain size is calculated using the full probability distribution associated with the polymer-solvent free energy, rather than merely using the value obtained from the minimum of the free energy. © *2005 American Institute of Physics*.
[DOI: 10.1063/1.1830435]

I. INTRODUCTION

The coil-globule transition was first predicted by Stockmayer[1] over four decades ago and was first observed experimentally by Tanaka and co-workers two decades later.[2,3] This phenomenon is the dramatic reduction in the average size of a single polymer chain in solution as the solvent conditions are changed from "good" to "poor." It remains a subject of intense experimental and theoretical interest, principally due to the qualitative similarity of this process to protein folding, one of the most important unsolved problems in molecular biology. A recent review by Baysal and Karasz[4] provides a thorough summary of the numerous studies carried out on the coil-globule transition.

Early theoretical studies of the collapse transition generally fall within one of two categories. On one hand, theories which follow the approach taken in the pioneering work by Flory[5] commence by constructing an expression for the polymer-solvent system free energy which is characterized by a single parameter describing the average physical size of the polymer coil. Numerous theoretical studies have employed this approach.[6–16] On the other hand, the theories of Lifshitz and co-workers[17–22] use a more complex order parameter of the spatial density distribution. More recently, the methodology of integral equation theories, originally developed to study liquids, has been employed to study polymer collapse[23–25] in a manner which uses the monomer-solvent and solvent-solvent interactions to calculate effective monomer-monomer pair interactions. In addition, rigorous calculations yielding exact results through a complete enumeration of polymer configurations have been applied to study the collapse transition, though they have been limited to very short chains and without direct incorporation of the solvent.[26–28]

Monte Carlo and molecular dynamics (MD) computer simulation methods have been used extensively to study the coil-globule transition. A large majority of these studies have employed implicit-solvent models, in that they consider isolated single polymer chains in which the influence of the solvent has been incorporated into effective monomer-monomer pair interactions.[29–53] Typically, these effective interactions are not derived from any specific solvent in a rigorous manner. Consequently, subtle effects arising, for example, from the packing of a specific solvent around the polymer, cannot be investigated with such an approach. The clear alternative is to employ simulation models which explicitly include the solvent particles. However, since an accurate description of a liquid solvent requires high solvent densities, the calculations unavoidably become extremely time consuming. While such calculations were unfeasible in the past, a number of studies of the coil-globule transition in the presence of an explicit solvent have been reported in recent years.[54–61] However, it is still not possible to study polymers of lengths that are anywhere near the limits possible for implicit-solvent models: typically, polymers in explicit-solvent simulation studies are 10^2 monomers in length or less, while simulations using polymer chains of 10^6 monomers have been reported in implicit-solvent studies.[34] An alternative, hybrid approach uses an implicit-solvent model polymer, but one in which the effective monomer-monomer interactions have been calculated directly from a specific solvent defined by monomer-solvent and solvent-

solvent interactions. Monte Carlo simulation employing the polymer reference interaction site model (PRISM theory) (Ref. 62) has proven to be a useful method of this type to study polymer collapse.[63–65] On the other hand, the principal advantage of this approach, namely, incorporating the solvent into effective monomer-monomer *pair* interactions using the hypernetted chain approximation, may constitute a rather severe approximation. As noted by Mendez *et al.*,[66] for example, the resulting pair potentials tend to have deep potential wells that lead to collapse under conditions where the swollen coil state should be stable. In addition, complicated effects due to many-body correlations cannot be accurately accounted for with such a model.[67] Consequently, explicit-solvent models remain the preferred route for studies of specific polymer-solvent systems wherever feasible.

In this study, we investigate the coil-globule transition of a polymer chain immersed in an explicit solvent using MD simulations. In light of the computational challenges described above, which are imposed by using such a model, we consider only a relatively short chain of 30 monomers. In addition, for computational convenience, we employ a model very similar to that used in Ref. 60: the model is characterized by a bead-spring model polymer, solvent particles that are the same size as the monomers, and monomers and solvent particles which each have only one interaction site. Clearly, the model is not designed to emulate any chemically specific polymer-solvent system; rather, we seek to elucidate the generic behavior of the collapse transition, with an emphasis on quantifying the effects of varying the solvent density. Extensive simulations were carried out to accurately trace out the coil-globule phase boundary. These results were then compared with a simple Flory-type theory for the polymer collapse transition in order to assess the range of validity of the various approximations employed in the theory.

Section II describes in detail the two different versions of the model polymer-solvent system employed in this study. Section III A describes the procedure used to accurately locate the coil-globule transition point, while Sec. III B outlines the theory used to compare with the calculated phase boundaries. The technical details of the MD simulations are then given in Sec. IV. Section V presents and discusses the main results of the study, and, finally, Sec. VI summarizes the key conclusions.

II. MODEL

We consider a three-dimensional system composed of a single linear fully flexible homopolymer chain immersed in an explicitly modeled solvent. For computational convenience, each solvent particle is chosen to have the same size and mass as the monomers on the polymer. Particle interactions are pairwise additive and depend on whether the particle is a monomer or a solvent particle. There are three distinct types of nonbonded pair interactions: the monomer-monomer potential u_{MM}, the monomer-solvent potential u_{MS}, and the solvent-solvent potential u_{SS}. In this study, we consider two different polymer-solvent model systems, henceforth referred to as models A and B, which are distinguished by the choice of these three nonbonded interactions.

In model A, the three interactions are given by

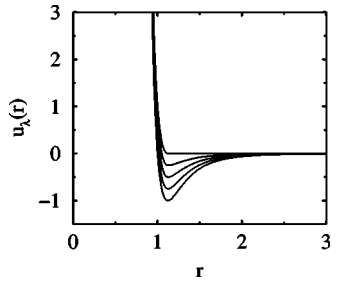

FIG. 1. The pair potential $u_\lambda(r)$ for values of $\lambda=0.0$, 0.25, 0.5, 0.75, and 1.0 from bottom to top.

$$
\begin{aligned}
u_{\mathrm{MM}}(r) &= u_{\mathrm{LJ}}(r), \\
u_{\mathrm{SS}}(r) &= u_{\mathrm{LJ}}(r), \\
u_{\mathrm{MS}}(r) &= u_{\lambda}(r),
\end{aligned}
\tag{1}
$$

where $u_{\mathrm{LJ}}(r)$ is a truncated and shifted Lennard-Jones (LJ) 6-12 potential

$$
\begin{aligned}
u_{\mathrm{LJ}}(r) &= u_{lj}(r) - u_{lj}(r_c), \quad r \leqslant r_c \\
&= 0, \quad r > r_c,
\end{aligned}
\tag{2}
$$

where

$$
u_{lj}(r) = 4\epsilon\left[\left(\frac{\sigma}{r}\right)^{12} - \left(\frac{\sigma}{r}\right)^{6}\right], \tag{3}
$$

where σ and ϵ are the usual LJ distance and energy parameters, respectively. We choose a cutoff distance of $r_c = 3\sigma$. Further, the potential $u_\lambda(r)$ is defined to be

$$
u_\lambda(r) = \lambda u_{\mathrm{rep}}(r) + (1-\lambda)u_{\mathrm{LJ}}(r), \tag{4}
$$

where the steeply repulsive interaction $u_{\mathrm{rep}}(r)$ is given by

$$
\begin{aligned}
u_{\mathrm{rep}}(r) &= u_{lj}(r) + \epsilon, \quad r \leqslant r_{\min} \\
&= 0, \quad r \geqslant r_{\min},
\end{aligned}
\tag{5}
$$

where $r_{\min} = 2^{1/6}\sigma$, corresponding to the minimum in the potential of Eq. (3). The parameter λ appearing in Eq. (4) is chosen to be in the range $\lambda \in [0,1]$.

Sample $u_\lambda(r)$ pair potentials are shown in Fig. 1 for $\lambda = 0.0$, 0.25, 0.5, 0.75, and 1.0 from bottom to top. Note that the bottom curve in the figure for $\lambda = 0$ corresponds to the LJ potential $u_{\mathrm{LJ}}(r)$ of Eq. (2), while the top curve corresponds to the potential $u_{\mathrm{rep}}(r)$ in Eq. (5). As seen in the figure, the effect of increasing λ is to decrease the depth of the potential well while maintaining the steeply repulsive component of the potential. The potentials have been designed, in part, so that an increase in λ will trigger a collapse transition. It is clear from a consideration of the choice of potentials in Eq. (1) that the globular state of the polymer will become more energetically favorable as λ increases. For this reason, the model parameter λ controls the degree of hydrophobicity of the polymer; consequently, we refer to λ as the hydrophobicity parameter.

In addition to the nonbonded interactions, there are interactions between pairs of bonded monomers. We choose a harmonic interaction of the form,

$$
u_b(r) = \tfrac{1}{2}k_b(r-l_0)^2, \tag{6}
$$

where k_b is the harmonic spring constant and l_0 is the equilibrium distance between bonded monomers. These parameters have values of $k_b\sigma^2/\epsilon=500$ and $l_0=\sigma$.

In model B, the nonbonded interactions are chosen to be

$$u_{\mathrm{MM}}(r)=u_{1-\lambda}(r),$$
$$u_{\mathrm{SS}}(r)=u_{\mathrm{rep}}(r), \tag{7}$$
$$u_{\mathrm{MS}}(r)=u_{\mathrm{rep}}(r),$$

where $u_{\mathrm{rep}}(r)$ is the repulsive interaction defined in Eq. (5). Further, $u_{1-\lambda}(r)$ is the potential given by Eq. (4) upon exchanging λ with $1-\lambda$. Consequently, the depth of the potential well associated with $u_{1-\lambda}(r)$ *increases* with increasing λ. Consideration of the potentials in Eq. (7) shows that increasing λ, as in model A, will increase the energy mismatch between monomers and solvent particles, and consequently make the globule state of the polymer increasingly energetically favorable. For this reason, λ is a measure of the polymer hydrophobicity for model B, as well.

The interaction between pairs of bonded monomers is identical to that of model A, given in Eq. (6).

All quantities described in this paper are given in Lennard-Jones reduced units. Specifically, distances are expressed in terms of σ, energies in terms of ϵ, temperature in terms of k_B/ϵ, where k_B is Boltzmann's constant, and time in terms of $\sqrt{m\sigma^2/\epsilon}$, where m is the mass of the each solvent particle and monomer. Further, the density of the system is defined to be the total particle number density, $\rho=(N+N_s)\sigma^3/V$, where V is the volume of the system.

III. BACKGROUND THEORY

A. Locating the transition

In the limit of sufficiently long chain length, the physical size of a polymer obeys the well-known scaling relation

$$R\sim N^{\nu}. \tag{8}$$

An important example of polymer size is the average radius of gyration of the polymer $\bar{R}_g$ defined as

$$\bar{R}_g\equiv\sqrt{\langle R_g^2\rangle}\equiv\sqrt{\frac{1}{N}\sum_{n=1}^{N}\langle|\vec{R}_n-\langle\vec{R}\rangle|^2\rangle}, \tag{9}$$

where $\vec{R}_n$ is the position of monomer n, $\langle\vec{R}\rangle$ is the average monomer position, N is the number of statistical segments of the polymer, and where the angular brackets denote a statistical averaging over polymer conformations. In the case of ideal chains, i.e., model chains with no interactions between nonbonded monomers, the scaling exponent is $\nu=1/2$. In so-called good solvent conditions, the scaling exponent is given by $\nu\approx0.588$.[68] In this case, the polymer chain is swollen; that is, it has a larger average physical size compared to that of an ideal chain, resulting from excluded volume interactions between monomers. This conformational state is often referred to as a "coil." Conversely, in so-called poor solvent conditions, the chain spans a smaller physical size compared to that of an ideal chain, and is characterized by a scaling exponent of $\nu=1/3$. If this collapsed state is liquidlike, as opposed to solidlike, then it is referred to as a "globule." Generally, the solvent conditions which determine the conformational state of a polymer in solution for a real physical system are determined by a complex interplay of the monomer-monomer, monomer-solvent, and solvent-solvent, interactions. The solvent conditions can be changed upon variation of various system properties (e.g., temperature, pH), which can then trigger a transition between the coil and globule states. A useful measure of the location of the transition is the so-called θ point, close to which the polymer behaves as though it were an ideal chain. In this study, we use the ideal-chain condition $\nu=1/2$ as an operational definition of the coil-globule transition. Note that this condition differs both from that for the true θ point, as well as from a more rigorously defined criterion for the collapse transition in the case of finite-length chains, as described below. Note, as well, that all three criteria converge in the limit of long chain length.

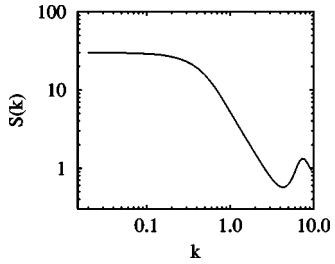

FIG. 2. Sample polymer static structure factor. The curve shown in the figure was obtained using the model A polymer-solvent model for a chain of length $N=30$ with a solvent density of $\rho=0.8$ and a hydrophobicity parameter of $\lambda=0$.

The static structure factor of a polymer chain can be used to determine the conformational state of a polymer chain. The structure factor is defined as

$$S(\vec{k})=\frac{1}{N}\sum_{n=1}^{N}\sum_{m=1}^{N}\langle\exp[i\vec{k}\cdot(\vec{R}_n-\vec{R}_m)]\rangle, \tag{10}$$

where $\vec{k}$ is the wave vector. For isotropic systems, the structure factor depends only on the magnitude of $\vec{k}$, and is given by

$$S(k)=\frac{1}{N}\sum_{m,n}\left\langle\frac{\sin[k|\vec{R}_m-\vec{R}_n|]}{k|\vec{R}_m-\vec{R}_n|}\right\rangle. \tag{11}$$

For the polymer chain considered in this study, the structure factor satisfies the relation

$$S(k)\propto k^{-1/\nu}, \tag{12}$$

in the limit where $R_g^{-1}\ll k\ll\sigma^{-1}$, where σ is simultaneously the monomer size and the bond length. Note that this condition is only satisfied for long chains, $N\gg1$, for which $R_g\gg\sigma$. In the present case, where $N=30$, the chains are too short to rigorously satisfy the condition. On the other hand, as is evident in the sample calculated structure factor plotted on the log-log graph in Fig. 2, there is a linear regime apparent in the range defined by the less rigid criterion $R_g^{-1}\lesssim k\lesssim\sigma^{-1}$. In this study we use the slope m of this linear regime to calculate the scaling exponent according to $\nu=-1/m$. While we expect there to be non-negligible finite-size ef-

fects, we expect the calculated coil-globule phase boundaries to display the general qualitative features present for longer-chain systems.

B. Comparing simulation results to theoretical predictions

Some understanding of the significance of the simulation results presented in this study can be gained from an analytical theoretical treatment of the polymer collapse transition. Here, we consider only the simple Flory–Huggins (FH) theory, in which the criterion for collapse is determined by the well-known Flory χ parameter, which in turn can be related to the parameters of the model polymer-solvent system. Two different procedures have been used to map the model parameters onto χ for each of the two polymer-solvent model systems. The details of these calculations are presented in this section.

The theoretical foundations of the coil-globule transition have been well established.[16,19–22,69] The two main classes of theories of the collapse transition follow the ideas of Flory[5] and Lifshitz.[70] In Flory-type theories of the collapse transition such as the one considered here, the polymer-solvent free energy is written in terms of a single order parameter, the expansion factor of the radius of gyration, while in Lifshitz-type theories, a more complex order parameter of the spatial density distribution is used. Following the approach of Flory, it can be shown that the free energy of a polymer-solvent system can be written approximately as follows:

$$F(\alpha)=F_{\mathrm{el}}(\alpha)+F_{\mathrm{int}}(\alpha), \tag{13}$$

where $F_{\mathrm{el}}(\alpha)$ is the elastic free energy of the ideal chain and where $F_{\mathrm{int}}(\alpha)$ is the contribution to the free energy from particle interactions. The expansion coefficient α is defined as

$$\alpha^2 \equiv R_g^2/\langle R_0^2\rangle \tag{14}$$

and where $\langle R_0^2\rangle$ is the average square radius of gyration of the corresponding ideal chain, i.e., in the absence of nonbonded interactions. An approximate expression for $F_{\mathrm{el}}(\alpha)$ is given by[16]

$$\begin{aligned}\beta F_{\mathrm{el}}(\alpha)&=\frac{9}{4}(\alpha^{-2}+2\ln\alpha), \quad \alpha>1\\ &=\frac{\pi^2}{4}(\alpha^2-2\ln\alpha), \quad \alpha<1.\end{aligned} \tag{15}$$

In the vicinity of the θ point, the chain is sufficiently large that the interaction term $F_{\mathrm{int}}(\alpha)$ can be written as

$$\beta F_{\mathrm{int}}(\alpha)=\left(\frac{B\sqrt{N}}{v}\right)\alpha^{-3}+\left(\frac{C}{v^2}\right)\alpha^{-6}, \tag{16}$$

where v is the excluded volume of each monomer. The first and second terms correspond to two- and three-body effects, respectively, arising from nonbonded interactions. Correspondingly, B and C refer to second- and third-order virial coefficients. Note that Eq. (16) is not expected to be valid in the regime of high compaction, i.e., in the globule state.

The average swelling coefficient $\bar{\alpha}\equiv\sqrt{\langle\alpha^2\rangle}$ is rigorously determined from the condition that

$$\bar{\alpha}^2=\langle\alpha^2\rangle=\frac{\int_0^\infty d\alpha\,\alpha^2\exp[-\beta F(\alpha)]}{\int_0^\infty d\alpha\exp[-\beta F(\alpha)]}. \tag{17}$$

Note that the discontinuity of $F_{\mathrm{el}}(\alpha)$ at $\alpha=1$ in Eq. (15) should be removed by shifting either function by the appropriate additive constant in order to employ it in the calculation of Eq. (17). On the other hand, for a sufficiently deep free energy minimum, $\bar{\alpha}$ is approximately given by the value of α which minimizes $F(\alpha)$, and which, from Eqs. (13), (15), and (16), is given by

$$\begin{aligned}\frac{\pi^2}{2}(\alpha^5-\alpha^3)&=\frac{3B\sqrt{N}}{v}+\frac{6C}{v^2}\alpha^{-3}, \quad \alpha\geqslant 1,\\ \frac{3}{2}(\alpha^3-\alpha)&=\frac{B\sqrt{N}}{v}+\frac{2C}{v^2}\alpha^{-3}, \quad \alpha\leqslant 1.\end{aligned} \tag{18}$$

In the limit of large N, Eq. (18) predicts a swollen-coil scaling exponent of $\nu=3/5$ for $B>0$, and a globule scaling exponent of $\nu=1/3$ for $B<0$. Thus, the θ point, defined to be the conditions under which $B=0$, marks the location of the coil-globule transition in the limit of large N. Note, however, that experimentally observed collapse transitions for finite-size polymers occurs at temperatures somewhat higher than the θ temperature. The origin of this discrepancy can be understood from a more rigorous treatment for the criterion for defining the collapse transition involving the balance between volume and surface contributions to the free energy of a globule.[69]

For each domain of α considered in Eq. (18) the condition that the chain behaves like an ideal chain ($\alpha=1$) yields the following criterion:

$$B=-\frac{2C}{v}N^{-1/2}. \tag{19}$$

Although the true polymer collapse transition, the θ point, and the ideal-chain condition all converge only in the limit $N\to\infty$, in this study, we will treat the $\alpha=1$ condition as an operational definition of the coil-globule transition.

For a polymer-solvent system at liquid-like solvent densities, it is natural to employ the FH form of the coefficients B and C:

$$B=v\left(\frac{1}{2}-\chi\right), \quad C=\frac{v^2}{6}. \tag{20}$$

In order to apply this theory to the simulation results of this study, we must choose a mapping between the off-lattice model employed in the simulations to the lattice model underlying the FH theory. For an off-lattice model, the simplest corresponding expression for the χ parameter can be written as

$$\chi=\Delta\epsilon/k_BT, \tag{21}$$

where the energy mismatch $\Delta\epsilon$ is given by

$$\Delta\epsilon=\bar{\epsilon}_{\mathrm{MS}}-\tfrac{1}{2}(\bar{\epsilon}_{\mathrm{SS}}+\bar{\epsilon}_{\mathrm{MM}}). \tag{22}$$

The energy terms are defined as

$$\bar{\epsilon}_{\alpha\beta}=\rho\int_0^\infty dr 4\pi r^2 g_{\alpha\beta}(r)u_{\alpha\beta}(r), \tag{23}$$

where $g_{\alpha\beta}(r)$ is the radial distribution function between particles of type α and β. We employ the simple random mixing approximation, whereby $g_{\mathrm{MM}}(r)=g_{\mathrm{MS}}(r)=g_{\mathrm{SS}}(r)\equiv g_\rho(r)$, where the subscript on $g_\rho(r)$ is included to emphasize that in general the distribution function will depend on the system particle density. For the models defined in Sec. II, the expression for χ can then be written as

$$\chi=\frac{2\lambda\epsilon\rho\sigma^3}{gk_BT}f(\rho), \tag{24}$$

where g is a numeric factor with a value of $g=2$ for model A and $g=1$ for model B, and where the dimensionless function $f(\rho)$ is defined as

$$f(\rho)\epsilon\sigma^3\equiv\int_0^\infty dr 4\pi r^2 g_\rho(r)[u_{\mathrm{rep}}(r)-u_{\mathrm{LJ}}(r)]. \tag{25}$$

In order to determine the function $f(\rho)$, we can make the rather drastic but convenient choice to extend the random mixing approximation in the dilute limit:

$$\begin{aligned} g_\rho(r)&=1 \quad \text{for} \quad r>\sigma \\ &=0 \quad \text{for} \quad r<\sigma. \end{aligned} \tag{26}$$

In this case, we find that $f(\rho)=a$, where the constant $a=10.391\,091$.

The collapse transition considered in this study is driven by variation of the hydrophobicity parameter λ defined for each of the models in Eq. (4). Thus, in the context of the present theory, variation in λ controls χ, and thus B, by changing the energy mismatch factor $\Delta\epsilon$. We refer to the value of λ that satisfies the θ condition in Eq. (19) as λ_θ. Using Eq. (20) and the expression for χ in Eq. (24) we can rewrite the criterion for the θ point in Eq. (19) as

$$\lambda_\theta=\frac{k_BT}{ag\rho\sigma^3\epsilon}\left(\frac{1}{2}+\frac{1}{3\sqrt{N}}\right). \tag{27}$$

In the limit of long chain length, $N\to\infty$, the second term in the round brackets vanishes, and this becomes the λ value corresponding to the collapse transition where $B=0$.

Another possible mapping between χ and λ is suggested in the paper by Mendez *et al.*,[66] who recently developed an integral equation theory for polymer solutions for the case of explicit inclusion of solvent particles. In this study, the PRISM theory is used to calculate pair radial distribution functions and an effective monomer-monomer pair potential describing the effects of purely repulsive interactions. In addition, the random phase approximation is used to build in the effects of the attractive components of the potentials in order to derive an expression for the spinodal condition for a binary system. The latter calculations also use the approximation that the monomer/solvent volume change on mixing at constant pressure is zero. Here, we consider a special case of the theory in which we assume that the polymer-solvent system is incompressible, and where we use the random mixing approximation, $g_{\alpha\beta}(r)=g_\rho(r)$ for $\alpha,\beta\in\mathrm{M,S}$. However, unlike the the mapping used to derive Eq. (27), no explicit form for $g_\rho(r)$ is assumed. Rather, it is determined by the expression for the spinodal condition which was derived in Ref. 71. Under these approximations, the Mendez *et al.* showed that the spinodal condition satisfies a form consistent with that appearing in the Flory–Huggins theory, with a χ parameter that can be calculated from the magnitudes of the attractive components of the various interparticle interactions. For the model systems considered in this study, this corresponds to a χ parameter given by

$$\chi=\frac{32\pi g\rho\sigma^3\epsilon\lambda}{9\sqrt{2}k_BT}, \tag{28}$$

where ρ is the total particle (solvent and monomer) number density, and where the factor g has values of $g=2$ for model A and $g=1$ for model B. The details of this calculation are presented in the Appendix. From Eq. (28), it is clear that this mapping is consistent with the expectation that λ controls the degree of hydrophobicity of the polymer. Using Eq. (20) and the expression for χ in Eq. (28) we can rewrite the criterion for the θ point in Eq. (19) as

$$\lambda_\theta=\frac{k_BT}{bg\rho\sigma^3\epsilon}\left(\frac{1}{2}+\frac{1}{3\sqrt{N}}\right), \tag{29}$$

where $b=(32\pi)/(9\sqrt{2})\approx 7.898\,459$.

Note that the expressions for λ_θ in Eqs. (27) and (29) have exactly the same form and differ solely in terms of the numeric prefactor. One consequence of this is that both theories predict that λ_θ is inversely proportional to the particle density of the system. Note further that each theory also predicts that the ratio of the values of λ_θ for the two models satisfy $r\equiv\lambda_\theta^{(B)}/\lambda_\theta^{(A)}=2$.

Four different procedures have been used to calculate theoretical coil-globule phase boundaries for each of the two model systems:

(I) Using Eq. (27). This employs the random mixing approximation in the dilute limit in Eq. (26) with Eq. (24) to relate λ to χ. In addition, it uses Eq. (19), which arises from minimizing the free energy defined by Eqs. (13), (15), and (16).

(II) Using Eq. (17) with the condition $\bar{\alpha}=1$, rather than Eq. (19), to impose the θ condition. Also, the same χ-λ mapping as in (I) is employed.

(III) Using Eq. (29). This employs the procedure outlined in the Appendix to derive the relation between λ and χ. In addition, it uses Eq. (19), which arises from minimizing the free energy defined by Eqs. (13), (15), and (16).

(IV) Using Eq. (17) with the condition $\bar{\alpha}=1$, rather than Eq. (19), to impose the θ condition. Also, the same χ-λ mapping as in (III) is employed.

IV. SIMULATION DETAILS

We employ constant-energy MD simulations to study the polymer-solvent model systems defined in Sec. II. We use a cubic simulation cell with standard periodic boundary conditions. The equations of motion were integrated using the

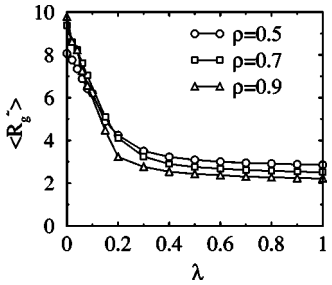

FIG. 3. $\langle R_g^2 \rangle$ vs model parameter λ for several densities for the model A polymer solvent system.

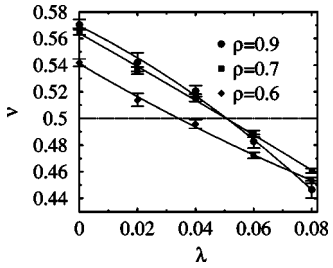

FIG. 4. Scaling exponent ν vs hydrophobicity parameter λ for the model A polymer-solvent system for three different solvent densities. The scaling exponents were obtained from an analysis of the static structure factor for the polymer chain. The solid lines are fits to a quadratic polynomial. The intersection of each of the fitted lines with the horizontal line at $\nu=0.5$ indicates the location of the θ point.

velocity-Verlet algorithm, with a time step of $\Delta t=0.005$. Verlet neighbor lists were used to improve the efficiency of the calculations. All simulations were carried out at a kinetic temperature of $T=1.0$. Velocity rescaling was used to set the temperature.

Most simulations employed polymers of length $N=30$ monomers immersed in a bath of N_s solvent particles, such that the total number of particles was $N+N_s=1000$. For any particular density, the monomers and solvent particles were initially placed on a cubic lattice. For convenience, the initial polymer chain conformation was composed of straight parallel segments along one face of the simulation cell wrapping through the periodic boundaries. The system was next equilibrated for a considerable time, $\Delta t_{\mathrm{eq}} \geqslant 2500-5000$, which was followed by a production run of $\Delta t=10\,000-20\,000$.

Individual simulations were carried out on the nodes of a 92-processor beowulf cluster with processor speeds ranging from 1.4–2.0 GHz, each requiring $\approx 24-48$ h of CPU time. Typically, average static structure factors were obtained from averaging the results of 10–12 simulations, each corresponding to the same system parameters, but with different initial conditions in order to achieve statistical independence. The average structure factor was then used to determine the scaling exponent ν. Typically, five to seven sets of these simulations for various values of the hydrophobicity parameter λ were used to determine the value of λ_θ, corresponding to a single point on a phase diagram for each of the two models. We emphasize that this constitutes an enormous computational effort, which was nevertheless required to obtain a sufficient level of statistical accuracy.

V. RESULTS AND DISCUSSION

We first consider the simulation results for the model A polymer-solvent system. Figure 3 shows the average square of the radius of gyration $\langle R_g^2 \rangle$ versus λ for four particle densities. As expected, an increase in λ clearly increases the hydrophobicity of the polymer and leads to a decrease in polymer size. For sufficiently low density, it is clear that the polymer exists only in the globule state. Further, the size of the polymer decreases monotonically for all λ with increasing particle density. This is consistent with theoretical predictions and simulation results for athermal polymer-solvent systems, and is due to entropy-induced effective attractive forces between monomers. These results are qualitatively consistent with those of the study by Polson and Zuckermann,[60] which used a model potential very similar to that used here.

Figure 4 shows the variation of the polymer scaling exponent ν with the hydrophobicity parameter λ for three of the ten solvent densities used in the simulations. Generally, there is a decrease in ν upon increasing λ. This decrease reflects the decrease in the polymer size brought about by increasing hydrophobicity of the polymer in the solvent. The horizontal dotted in line in the figure indicates the θ condition where $\nu=1/2$. For each case, the system changes from better-than-θ to worse-than-θ conditions as λ increases. Each dataset has been fit to a quadratic polynomial, which is shown as the solid lines in the figure. The value of λ_θ was found by determining where the quadratic polynomial satisfies the θ criterion; equivalently, it is the location where the curves intersect the dotted line in the figure.

The case of $\lambda=0$ corresponds to the hydrophilic limit in this model system. In this limit, all nonbonded interactions are given by the truncated LJ potential in Eq. (2). Thus, there is no energy mismatch between the monomers and solvent particles. From the figure, we note that the scaling exponent ν is consistently lower than the universal good-solvent value of $\nu \approx 0.588$. There are probably two main reasons for this feature. First, it is fully expected that there will be finite-size effects as a result of the relatively short chain ($N=30$) employed in these calculations, as the theoretical value is strictly valid in the long chain limit. It is likely that the measured value of ν will approach the theoretical value for longer chains. However, this will only be the case at higher solvent densities. Note that we have employed a temperature of $T=1$ where an isolated (i.e., at $\rho=0$) LJ polymer chain is in the collapsed globule state. At sufficiently high ρ the attractive monomer-monomer interactions are effectively screened by the LJ solvent; however, the screening weakens as the solvent becomes more dilute. Consequently, even in the hydrophilic limit of $\lambda=0$ we expect the solvent conditions to worsen with decreasing solvent density. This fact also accounts in part for the low values of ν at $\lambda=0$.

Table I lists the measured values of λ_θ for each density. Figure 5 shows the corresponding phase diagram in the ρ-λ plane. We find that the location of the transition is ρ independent for $\rho \gtrsim 0.65$, but occurs at λ_θ which decrease ap-

TABLE I. Calculated λ_θ for each particle density for model A and model B.

Model A		Model B	
ρ	λ_θ	ρ	λ_θ
0.4448 ± 0.0054	0		
0.50	0.0126 ± 0.0021	0.0	0.4124 ± 0.0019
0.55	0.0273 ± 0.0017	0.2	0.2834 ± 0.0019
0.60	0.0342 ± 0.0017	0.3	0.2440 ± 0.0018
0.65	0.0496 ± 0.0011	0.4	0.2158 ± 0.0017
0.70	0.0506 ± 0.0011	0.5	0.1835 ± 0.0015
0.75	0.0527 ± 0.0012	0.6	0.1496 ± 0.0021
0.80	0.0532 ± 0.0020	0.7	0.1276 ± 0.0023
0.85	0.0512 ± 0.0026	0.8	0.1112 ± 0.0025
0.90	0.0507 ± 0.0016	0.9	0.1014 ± 0.0027

proximately linearly with decreasing ρ. The minimum solvent density at which the coil can exist occurs at $\rho \approx 0.45$. Likewise the maximum solvent density for which the coil is possible occurs at $\lambda \approx 0.05$; thus, the collapse transition can be driven by a decrease in solvent density for $\lambda \in [0,0.05]$.

The physically meaningful regime corresponds to the high-ρ limit, corresponding to the case of liquidlike densities. The ρ independence of the transition in this regime is a noteworthy feature that merits some comment. First, we note that the coil-globule transition is mainly driven by a competition between the system energy, which increasingly favors the globule state at high λ, and the configurational entropy of the chain, which favors the coil state. However, at high ρ, the effects of the translational entropy of the solvent are expected to become more significant. Simulation[54–56,58,72] and theoretical[24,64–66,73] studies of athermal polymer-solvent systems suggest that the explicit presence of the solvent induce effective attractive forces between monomers which can trigger a collapse of the polymer for sufficiently high solvent density. Essentially, this means that the degree to which the solvent entropy favors the globule state increases with ρ. To our knowledge, such an entropic collapse transition has never been observed in simulations using off-lattice models,[74] possibly because it is preempted by the freezing transition of the solvent. On the other hand, it is conceivable that such solvent-induced effective attractions in the present (i.e., not athermal) system could influence the location and

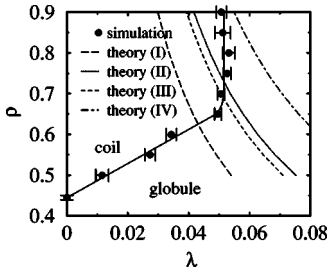

FIG. 5. Phase diagram of the model A polymer-solvent system in terms of solvent density ρ and hydrophobicity parameter λ. The coil-globule phase boundary is constructed from data points obtained from the condition that the scaling exponent satisfies the θ condition $\nu = 0.5$. The solid line is included as a guide for the eye. As explained in Sec. III B, the four theoretical phase boundaries have been calculated as follows: (I) Eq. (27); (II) using Eq. (17) with the condition that $\bar{\alpha} = 1$ and Eq. (24); (III) using Eq. (29); (IV) using Eq. (17) with the condition that $\bar{\alpha} = 1$ and Eq. (28).

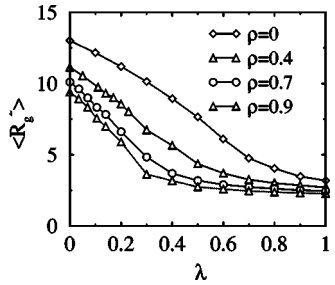

FIG. 6. $\langle R_g^2 \rangle$ vs model parameter λ for several densities for the model B polymer solvent system.

character of the phase boundary at high ρ. Specifically, we would anticipate that the globule state would be increasingly favored at high ρ, thus shifting the boundary to lower λ with increasing ρ. If such a feature is present, it is masked by the statistical uncertainties of the data.

The theoretical predictions of the coil-globule phase boundary presented in Sec. III B were applied to the model A polymer-solvent system. Four different calculations were performed, as described at the end of Sec. III B. As explained in that section, the calculations differ by choice in the mapping between λ and χ, and by whether or not fluctuations about the minimum in the free energy $F(\alpha)$ are accounted for. The theoretical curves in Fig. 5 are labeled in a manner consistent with the listing in Sec. III B. At first glance, all predictions appear to be extremely poor. The prediction that $\lambda_\theta \propto \rho^{-1}$ is evident in the figure and is in qualitative disagreement with with the fact that the measured λ_θ is ρ independent for higher densities ($\rho \gtrsim 0.65$) and *increases* with increasing ρ at lower densities ($0.45 < \rho \lesssim 0.65$). However, this discrepancy is entirely expected, and can be at least partially understood from the fact that the mapping of the model parameters onto the χ parameter in each version of the FH theory uses the assumption that the polymer-solvent system is incompressible, and thus that there are are no density fluctuations. For this reason, the predictions should only be expected to be accurate in the limit of high particle density, where the density fluctuations are expected to be very small. As is evident in the figure, the agreement between theory and simulation is indeed considerably better at high densities. Consequently, a proper test of the theory is the degree to which the predicted phase boundary converges to that of the simulation in the limit of high density. It is noteworthy that the predictions that use the free energy minimum condition implicit in Eq. (19) are generally poorer than those which use Eq. (17) together with the criterion $\bar{\alpha} = 1$ to impose the θ condition. This result is qualitatively consistent with the fact that using Eq. (17) to account for fluctuations about the free energy minimum provides the more accurate approach to determine $\bar{\alpha}$. For longer polymer chains, it is expected that the predictions from the two methods for determining α will converge. However, for the short $N = 30$ chain considered here, the two predictions are noticeably different. On the other hand, Fig. 5 also demonstrates that the two mappings between χ and λ given in Eqs. (27) and (29) yield predictions which are accurate to a quantitatively comparable degree.

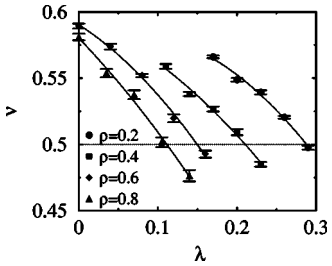

FIG. 7. Scaling exponent ν vs hydrophobicity parameter λ for the model B polymer-solvent system for four different solvent densities. The scaling exponents were obtained from an analysis of the static structure factor for the polymer chain. The solid lines are fits to a quadratic polynomial. The intersection of each of the fitted lines with the horizontal line at $\nu=0.5$ indicates the location of the θ point.

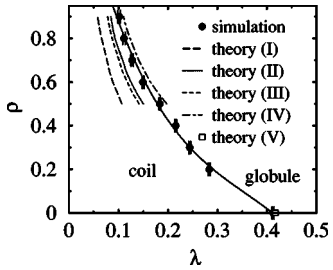

FIG. 8. Phase diagram of the Model B polymer-solvent system in terms of solvent density ρ and hydrophobicity parameter λ. The coil-globule phase boundary is constructed from data points (solid circles) obtained from the condition that the scaling exponent satisfies the θ condition $\nu=0.5$. The solid line is included as a guide for the eye. As explained in Sec. III B, the four theoretical phase boundaries have been calculated as follows: (I) Eq. (27); (II) using Eq. (17) with the condition that $\bar{\alpha}=1$ and Eq. (24); (III) using Eq. (29); (IV) using Eq. (17) with the condition that $\bar{\alpha}=1$ and Eq. (28). In addition, the single point labeled (V) shows the theoretical prediction for zero solvent density, which was obtained from direct evaluation of the free energy virial coefficients appearing in the θ criterion in Eq. (19), using monomer-monomer interactions.

We now consider the results for the model B polymer-solvent model system. Figure 6 shows the average square of the radius of gyration $\langle R_g^2 \rangle$ versus λ for four particle densities. As expected, an increase in λ clearly increases the hydrophobicity of the polymer and leads to a decrease in polymer size. The transition is somewhat broad, as a result of the short chain considered here. Further, the size of the polymer decreases monotonically for all λ with increasing particle density. This is consistent with theoretical predictions and simulation results for athermal polymer-solvent systems, and is due to entropy-induced effective attractive forces between monomers.

Figure 7 shows the variation of the scaling exponents with λ for several different solvent densities. Again, we note that increasing λ clearly increases the degree of the polymer hydrophobicity as manifested by the corresponding decrease in ν. As in Fig. 4, the datasets have been fit to a quadratic polynomial, also shown in this figure. The intersection of the fitting curves with the dotted line, corresponding to the value of $\nu=1/2$ marks the location of λ_θ for each density. Unlike the case in model A, we note that λ_θ consistently increases as the solvent density decreases. Consequently, the coil state was observed for sufficiently low λ for over the full range of solvent densities considered, $\rho \in [0,0.9]$. This is clearly evident in Fig. 8, which shows the model-B phase diagram in the ρ-λ plane. The basic features of the phase diagram can be understood easily upon consideration of the features of the model. As specified in Eq. (7), at $\lambda=0$, the monomer-monomer interactions are solely repulsive in nature. Consequently, in the absence of a solvent there is no mechanism driving the polymer to collapse, and thus the isolated polymer ($\rho=0$) exists in the coil state, unlike the case in model A, where the attractive monomer-monomer interactions induced a globule state at the temperature used. As specified as well in Eq. (7), monomer-solvent and solvent-solvent interactions are also purely repulsive, independent of λ. As mentioned above, no entropy-driven collapse transition has been observed for repulsive additive-potential polymer-solvent model systems. Thus, the polymer exists in the swollen coil state for the full range of solvent densities. On the other hand, increasing λ increases the depth of the monomer-monomer potential wells, which, for the temperature of $T=1$ considered here, is sufficient to drive a collapse transition. Thus, the coil-globule transition occurs for all densities considered upon increasing λ.

The most interesting feature of the model B phase diagram is the monotonic shift of the phase boundary to lower λ upon an increase in solvent density. Thus, an increase in ρ enhances the stability of the globule over the coil state. This trend is qualitatively consistent with the prediction that increasing solvent density will increase the solvent-induced attractions between monomers.

The theoretical approach of Sec. III B was also applied to model B. We consider the same four methods for determining λ_θ as were used in the analysis of the phase diagram for model A. The predicted phase boundaries are all shown in Fig. 8. In contrast to the case for model A, the predicted phase boundaries do not diverge significantly from the true boundary as the particle density decreases; rather, the difference between the two stays roughly constant. However, it should not be inferred that the theory is inherently more accurate for model B. At lower particle densities, the system is far from the incompressible limit, a condition assumed in the Flory-type theories considered here. The physical origin of the increase in the stability of the globule state with increasing solvent density is almost certainly due the entropy-induced effective interactions between monomers, which are known to increase with density. This effect is expected to be enhanced somewhat by the slight nonadditivity of the repulsive cores of the different potentials, as is evident from Fig. 1, the effects of which has been studied in Ref. 58. By contrast, the observed decrease of λ_θ with ρ arises from the fact that $\chi \propto \rho$ in Eqs. (27) and (29), which in turn arises from the assumed purely enthalpic form of χ implicit in the theory. Consequently, it is still only in the limit of high density where the predictions are expected to be more accurate. As in the case of the predictions for model A, Fig. 8 demonstrates that the theoretical curves calculated using Eq. (17) to impose the θ condition are more accurate than those calculated using Eq. (19). Again, this difference is expected, though it is also expected to diminish with increasing polymer chain length. Also, there is no appreciable difference in the accu-

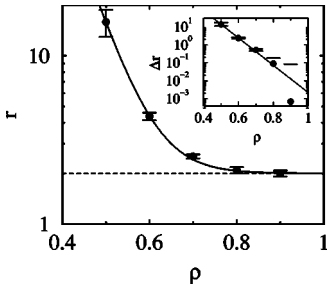

FIG. 9. Ratio $r \equiv \lambda_\theta^{(B)}(\rho)/\lambda_\theta^{(A)}(\rho)$ vs solvent density. The horizontal dashed line corresponding to $r=2$ corresponds to the theoretical predictions in both Eqs. (27) and (29). The solid line is an exponential fit to the data. The inset shows the same data ($\Delta r \equiv r-2$) and fit on a semilog scale.

racy of the predictions from the χ-λ mappings in Eqs. (27) and (29).

Figure 9 shows the density dependence of the ratio of the values of λ_θ for the two models, $r \equiv \lambda_\theta^{(B)}/\lambda_\theta^{(A)}$. The ratio is large at low ρ, but rapidly converges to a value of $r=2$ at high ρ. This is exactly the predicted value for the versions of the Flory-type theory considered here. More specifically, it is the value predicted by a Flory theory when the random mixing approximation $[g_{\mathrm{MM}}(r)=g_{\mathrm{MS}}(r)=g_{\mathrm{SS}}(r)\equiv g(r)]$ is invoked, together with the assumption that the radial distribution function is *identical* for both models. This intriguing result is hard to reconcile with the fact that the random mixing approximation is not expected to be particularly accurate. On the other hand, it seems unlikely to be merely a coincidence, but rather is likely a consequence of a more general, less restrictive criterion. In addition, it is clear from the figure that r exhibits an exponential decay; that is, $\Delta r \equiv r-2 \propto \exp(-\kappa\rho)$. The decay constant is determined to be $\kappa = 17.5071$. The physical significance of this last observation is not clear, assuming there is any at all.

The model systems considered in this study have employed a polymer of length $N=30$ in a solvent of N_s solvent particles such that the total particle number is $N_{\mathrm{tot}}=N+N_s=1000$. This results in relatively small simulation cell size at the higher densities. Near the θ point and at high ρ, the cell size l_c is typically $l_c \approx 4R_g$. Ideally, the cell size should be much larger than R_g in order to minimize possible finite-size effects. Unfortunately, this would also lead to simulations that are considerably more time consuming than the already computationally intensive simulations carried out for this study. However, to gain some degree of insight into the quantitative effects of increasing the cell size, a few select additional simulations were carried out for model B at a density of $\rho=0.8$ for system sizes of $N_{\mathrm{tot}}=12^3$, 14^3, and 16^3.

TABLE II. Measured λ_θ for the model B system at a particle density of $\rho=0.8$ for a polymer of length $N=30$ for various values total particle number $N_{\mathrm{tot}} \equiv N+N_s$, where N_s is the total number of solvent particles.

N_{tot}	λ_θ
1000	0.1112 ± 0.0025
1728	0.1146 ± 0.0037
2744	0.1167 ± 0.0043
4096	0.1132 ± 0.0031

The calculated values of λ_θ are listed in Table II. Within the statistical uncertainties, there is no significant difference in the locations of the θ point for the different systems.

VI. CONCLUSIONS

Two simple polymer-solvent model systems were employed to study the coil-globule transition. In each case, the transition is driven by a change in a model parameter λ which generates an energy mismatch between monomers and solvent particles. The polymer scaling exponent ν was determined from a measurement of the static structure factor in order to determine the θ-point separating the coil from the globule. The calculated coil-globule phase boundaries were compared with those predicted from a Flory-type theory using the free energy $F(\alpha)$ with and without fluctuations about the free energy minimum, and two different methods to map the model parameter λ onto χ. The theories are only expected to be valid at high densities, near the incompressible limit. Generally, it was found that the predictions were quantitatively more accurate for the case where α was determined using the full probability distribution associated with the free energy, rather than from the condition of minimum free energy. This effect arises as a result of the short chain ($N=30$) that was used in the simulations. On the other hand, neither of the χ-λ mappings lead to significantly more accurate predictions. Finally, it was noted that the ratio of the λ_θ values for the two models at high ρ was precisely that predicted by the Flory theory under the random mixing approximation and with the identical radial distribution functions for the two models. This is somewhat surprising given the crudeness of the random mixing approximation.

Some attempt has been made to address the issue of finite-size effects in this study by considering the effects of using larger simulation cell sizes. On the other hand, all simulations have used relatively short ($N=30$) polymer chains. It is not clear how the coil-globule phase boundary would be affected by increasing chain length. We believe it to be unlikely that the qualitative features of the phase diagrams would change; however, a careful study involving scaling N would greatly help to resolve this matter. Another noteworthy limitation of the models is the use of solvent particles which are the same size as the monomers. It would be very useful to investigate systems with smaller solvent-to-monomer size ratios, as this more accurately describes the polymer-solvent systems in experimental studies of polymer collapse. Finally, although the simple models employed here are sufficient to test theoretical predictions of polymer collapse, a more realistic description of the various pair interactions would provide better contact with experimental results.

The Flory-type theory of polymer collapse used in this study is a simple mean-field theory which should not be expected to yield particularly accurate predictions. In fact, the theory performed relatively well in the high density limit. Still, it would be advantageous to revisit the analysis of the simulation results using more sophisticated theories of polymers in solution that are designed to be applicable over a wider range of solvent densities.

ACKNOWLEDGMENTS

The authors thank Sheldon Opps for stimulating discussions and for a critical reading of this manuscript. The authors also wish to acknowledge the financial support of the Natural Sciences and Engineering Research Council of Canada and the Canada Foundation for Innovation.

APPENDIX: RELATION BETWEEN χ AND THE MODEL PARAMETER λ

In this appendix, the theory developed in Ref. 66 is used to derive the relation mapping the model parameter λ onto the Flory–Huggins χ parameter written in Eq. (29). The theory in that study is an extension of the PRISM integral equation theory developed by Curro and Schweizer.[62,75–78] Specifically, the PRISM theory was modified to allow for the explicit inclusion of the solvent particles. They consider a bead-spring flexible polymer in a monomeric solvent. Lennard-Jones (LJ) 6-12 interactions between sites are decomposed into repulsive and attractive interactions, the latter of which given by

$$u_{\alpha\gamma}^{\mathrm{att}}(r)=4\epsilon_{\alpha\gamma}^{\mathrm{att}}\left[\left(\frac{\sigma_{\alpha\gamma}}{r}\right)^{12}-\left(\frac{\sigma_{\alpha\gamma}}{r}\right)^{6}\right], \tag{A1}$$

in the regime $r\geqslant 2^{1/6}\sigma_{\alpha\gamma}$, where r is the distance between sites α and γ. The generalized LJ parameter $\epsilon_{\alpha\gamma}^{\mathrm{att}}$ corresponds to the strength of attraction between the sites, while $\sigma_{\alpha\gamma}$ is related to the size of the two interacting particles. Using an exact expression for the spinodal condition of a compressible binary system,[71] an expression for the spinodal temperature was obtained [see Eq. (13) of Ref. 66]. Imposing the incompressibility constraint, as well as the random mixing approximation, in which the monomer-monomer, monomer-solvent, and solvent-solvent radial distribution functions are taken to be equal, the expression for the spinodal temperature reduces to a form consistent with that predicted by Flory–Huggins theory,

$$k_BT_S=\frac{64\pi\sigma^3\rho}{9\sqrt{2}}\frac{\Delta\epsilon}{[1/xN+1/(1-x)]}, \tag{A2}$$

where x is the site fraction of the polymer, and where

$$\Delta\epsilon\equiv\epsilon_{\mathrm{mm}}^{\mathrm{att}}+\epsilon_{\mathrm{ss}}^{\mathrm{att}}-2\epsilon_{\mathrm{ms}}^{\mathrm{att}}. \tag{A3}$$

This corresponds to a χ parameter given by

$$\chi=\frac{32\pi\sigma^3\rho}{9\sqrt{2}}\frac{\Delta\epsilon}{k_BT}. \tag{A4}$$

In order to employ Eq. (4) in the theory of Sec. III B, the parameters $\epsilon_{\mathrm{mm}}^{\mathrm{att}}$, $\epsilon_{\mathrm{ms}}^{\mathrm{att}}$, and $\epsilon_{\mathrm{ss}}^{\mathrm{att}}$ must be related to the parameters appearing in the two models of this study. We choose the minimum energies of the pair potentials in Eq. (1) for model A and in Eq. (7) for model B to assign these parameters. We note that the depth of the potential energy minimum in the potential $u_\lambda(r)$ for model A and for $u_{1-\lambda}(r)$ for model B is given by $(1-\lambda)\epsilon$ and $\lambda\epsilon$, respectively. Consequently, for model A, $\epsilon_{\mathrm{mm}}^{\mathrm{att}}=\epsilon_{\mathrm{ss}}^{\mathrm{att}}=\epsilon$ and $\epsilon_{\mathrm{ms}}^{\mathrm{att}}=(1-\lambda)\epsilon$, which yields $\Delta\epsilon=2\lambda\epsilon$. Likewise, for model B, $\epsilon_{\mathrm{ms}}^{\mathrm{att}}=\epsilon_{\mathrm{ss}}^{\mathrm{att}}=0$ and $\epsilon_{\mathrm{mm}}^{\mathrm{att}}=\lambda\epsilon$, which yields $\Delta\epsilon=\lambda\epsilon$. Consequently, we can write

$$\chi=\frac{32\pi g\rho\sigma^3\epsilon\lambda}{9\sqrt{2}k_BT}, \tag{A5}$$

where the constant g has values of $g=2$ for model A and $g=1$ for model B.

[1] W. H. Stockmayer, Macromol. Chem. Phys. **35**, 54 (1960).
[2] I. Nishio, S.-T. Sun, G. Swislow, and T. Tanaka, Nature (London) **281**, 208 (1979).
[3] G. Swislow, S.-T. Sun, I. Nishio, and T. Tanaka, Phys. Rev. Lett. **44**, 796 (1980).
[4] B. M. Baysal and F. E. Karasz, Macromol. Theory Simul. **12**, 627 (2003).
[5] P. J. Flory, *Principles of Polymer Chemistry* (Cornell University Press, Ithaca, NY, 1953).
[6] O. B. Ptitsyn and E. Eizner, Biophys. USSR **10**, 1 (1965).
[7] O. B. Ptitsyn, A. K. Kron, and E. Y. Eizner, J. Polym. Sci., Part C: Polym. Symp. **16**, 3509 (1968).
[8] E. Y. Eizner, Polym. Sci. U.S.S.R. **11**, 409 (1969).
[9] P.-G. de Gennes, J. Phys. (Paris), Lett. **36**, L55 (1975).
[10] I. Sanchez, Macromolecules **12**, 980 (1979).
[11] E. A. di Marzio, Macromolecules **17**, 969 (1984).
[12] M. Muthukumar, J. Chem. Phys. **81**, 6272 (1984).
[13] G. Allegra and F. Ganazzoli, Macromolecules **16**, 1317 (1983).
[14] G. Allegra and F. Ganazzoli, J. Chem. Phys. **83**, 397 (1987).
[15] J. Des Cloiseaux and G. Jannink, *Polymers in Solution* (Oxford University Press, Oxford, UK, 1991).
[16] T. M. Birshtein and V. A. Pryamitsyn, Macromolecules **24**, 1554 (1991).
[17] I. M. Lifshitz, A. Y. Grosberg, and A. R. Khokhlov, Rev. Mod. Phys. **50**, 683 (1978).
[18] A. Y. Grosberg and A. R. Khokhlov, Sov. Sci. Rev., Sect. A **8**, 147 (1987).
[19] A. Y. Grosberg and D. V. Kuznetsov, Macromolecules **25**, 1970 (1992).
[20] A. Y. Grosberg and D. V. Kuznetsov, Macromolecules **25**, 1980 (1992).
[21] A. Y. Grosberg and D. V. Kuznetsov, Macromolecules **25**, 1991 (1992).
[22] A. Y. Grosberg and D. V. Kuznetsov, Macromolecules **25**, 1996 (1992).
[23] M. P. Taylor and J. E. G. Lipson, J. Chem. Phys. **104**, 4835 (1996).
[24] H. H. Gan and B. C. Eu, J. Chem. Phys. **109**, 2011 (1998).
[25] H. H. Gan and B. C. Eu, J. Chem. Phys. **110**, 3235 (1999).
[26] M. P. Taylor, Mol. Phys. **86**, 73 (1995).
[27] M. P. Taylor, J. Chem. Phys. **114**, 6472 (2001).
[28] M. P. Taylor, J. Chem. Phys. **118**, 883 (2003).
[29] N. Karasawa and W. A. Goddard III, J. Phys. Chem. **92**, 5828 (1988).
[30] I. Szleifer, E. M. O'Toole, and A. Z. Panagiotopoulos, J. Chem. Phys. **97**, 6802 (1992).
[31] A. Milchev, W. Paul, and K. Binder, J. Chem. Phys. **99**, 4786 (1993).
[32] T. A. Kavassalis and P. R. Sundararajan, Macromolecules **26**, 4144 (1993).
[33] P. Grassberger and R. Hegger, J. Chem. Phys. **102**, 6881 (1995).
[34] P. Grassberger, Phys. Rev. E **56**, 3682 (1997).
[35] A. M. Rubio, J. J. Freire, J. H. R. Clarke, C. W. Wong, and M. Bishop, J. Chem. Phys. **102**, 2277 (1995).
[36] J. Ma, J. E. Straub, and E. I. Shakhnovich, J. Chem. Phys. **103**, 2615 (1995).
[37] G. Tanaka and W. L. Mattice, Macromolecules **28**, 1049 (1995).
[38] G. Tanaka and W. L. Mattice, Macromol. Theory Simul. **5**, 499 (1996).
[39] M. Wittkop, S. Kreitmeier, and D. Göritz, J. Chem. Phys. **104**, 3373 (1996).
[40] Y. Zhou, M. Karplus, J. M. Wichert, and C. K. Hall, J. Chem. Phys. **107**, 10691 (1997).
[41] J. P. K. Doye, R. P. Sear, and D. Frenkel, J. Chem. Phys. **108**, 2134 (1998).
[42] W. Hu, J. Chem. Phys. **109**, 3686 (1998).
[43] H. Noguchi and K. Yoshikawa, J. Chem. Phys. **109**, 5070 (1998).
[44] V. A. Ivanov, W. Paul, and K. Binder, J. Chem. Phys. **109**, 5659 (1998).
[45] Q. Liao and X. Jin, J. Chem. Phys. **110**, 8835 (1999).
[46] A. Irbäck and E. Sandelin, J. Chem. Phys. **110**, 12256 (1999).
[47] P.-Y. Lai, Macromol. Theory Simul. **8**, 382 (1999).
[48] H. Liang and H. Chen, J. Chem. Phys. **113**, 4469 (2000).
[49] V. A. Ivanov, M. R. Stukan, V. V. Vasilevskaya, W. Paul, and K. Binder, Macromol. Theory Simul. **9**, 488 (2000).
[50] S. Fujiwara and T. Sato, J. Chem. Phys. **114**, 6455 (2001).

[51] W. Paul and M. Müller, J. Chem. Phys. **115**, 630 (2001).
[52] F. Calvo, J. P. K. Doye, and D. J. Wales, J. Chem. Phys. **116**, 2642 (2002).
[53] L. Huang, X. He, Y. Wang, H. Chen, and H. Liang, J. Chem. Phys. **119**, 2432 (2003).
[54] M. Dijkstra, D. Frenkel, and J.-P. Hansen, J. Chem. Phys. **101**, 3179 (1994).
[55] M. Dijkstra and D. Frenkel, Phys. Rev. Lett. **72**, 298 (1994).
[56] J. K. C. Suen, F. A. Escobedo, and J. J. de Pablo, J. Chem. Phys. **106**, 1288 (1997).
[57] V. V. Vasilevskaya, P. G. Khalatur, and A. R. Khokhlov, J. Chem. Phys. **109**, 5119 (1998).
[58] J. M. Polson, Phys. Rev. E **60**, 3429 (1999).
[59] J. M. Polson and M. J. Zuckermann, J. Chem. Phys. **113**, 1283 (2000).
[60] J. M. Polson and M. J. Zuckermann, J. Chem. Phys. **116**, 7244 (2002).
[61] C. F. Abrams, N. K. Lee, and S. P. Obukhov, Europhys. Lett. **59**, 391 (2002).
[62] K. S. Schweizer and J. G. Curro, Adv. Chem. Phys. **98**, 1 (1997).
[63] V. V. Vasilevskaya, P. G. Khalatur, and A. R. Khokhlov, J. Chem. Phys. **109**, 5108 (1998).
[64] P. G. Khalatur and A. R. Khokhlov, Mol. Phys. **93**, 555 (1998).
[65] P. G. Khalatur, L. V. Zherenkova, and A. R. Khokhlov, Eur. Phys. J. B **5**, 881 (1998).
[66] S. Mendez, J. G. Curro, M. Pütz, D. Bedrov, and G. D. Smith, J. Chem. Phys. **115**, 5669 (2001).
[67] C. J. Grayce, J. Chem. Phys. **106**, 5171 (1997).
[68] A. Sokal, in *Monte Carlo and Molecular Dynamics Simulation in Polymer Science*, edited by K. Binder (Oxford University Press, Oxford, 1995).
[69] A. Y. Grosberg and A. R. Khokhlov, *Statistical Physics of Macromolecules*, AIP Series in Polymers and Complex Materials (AIP, New York, 1994).
[70] I. M. Lifshitz, Sov. Phys. JETP **28**, 1280 (1969).
[71] J. G. Curro and K. S. Schweizer, Macromolecules **24**, 6736 (1991).
[72] G. Luna-Bárcenas, J. C. Meredith, I. C. Sanchez, K. P. Johnston, D. G. Cromov, and J. J. de Pablo, J. Chem. Phys. **107**, 10782 (1997).
[73] P. van der Schoot, Macromolecules **31**, 4635 (1998).
[74] Strictly speaking, such a transition was observed in the study of Ref. 56. However, a collapse transition was observed only in the case where the ''solvent'' particle diameter was close to the radius of gyration of the polymer in the coil state. An entropy-driven transition was observed for a nonadditive-potential polymer-solvent model in Ref. 58.
[75] K. S. Schweizer and J. G. Curro, Phys. Rev. Lett. **58**, 246 (1987).
[76] J. G. Curro and K. S. Schweizer, Macromolecules **20**, 1928 (1987).
[77] J. G. Curro and K. S. Schweizer, J. Chem. Phys. **87**, 1842 (1987).
[78] K. S. Schweizer and J. G. Curro, Adv. Polym. Sci. **116**, 321 (1994).